J. Fluid Mech. (2009), *vol.* 629, *pp.* 73–85.
doi:10.1017/S0022112009006594 Printed in the United Kingdom

A regularized model for strongly nonlinear internal solitary waves

WOOYOUNG CHOI[1]†, RICARDO BARROS[1] AND TAE-CHANG JO[2]

[1]Department of Mathematical Science, Center for Applied Mathematics and Statistics, New Jersey Institute of Technology, Newark, NJ 07102, USA

[2]Department of Mathematics, Inha University, Incheon 402-751, Korea

(Received 24 October 2008 and in revised form 30 January 2009)

The strongly nonlinear long-wave model for large amplitude internal waves in a two-layer system is regularized to eliminate shear instability due to the wave-induced velocity jump across the interface. The model is written in terms of the horizontal velocities evaluated at the top and bottom boundaries instead of the depth-averaged velocities, and it is shown through local stability analysis that internal solitary waves are locally stable to perturbations of arbitrary wavelengths if the wave amplitudes are smaller than a critical value. For a wide range of depth and density ratios pertinent to oceanic conditions, the critical wave amplitude is close to the maximum wave amplitude and the regularized model is therefore expected to be applicable to the strongly nonlinear regime. The regularized model is solved numerically using a finite-difference method and its numerical solutions support the results of our linear stability analysis. It is also shown that the solitary wave solution of the regularized model, found numerically using a time-dependent numerical model, is close to the solitary wave solution of the original model, confirming that the two models are asymptotically equivalent.

1. Introduction

Theoretical modelling of large amplitude internal solitary waves observed frequently in density-stratified coastal oceans is a challenging task. The ratio of wave amplitude to characteristic vertical length scale such as the thickness of the upper mixed layer is typically $O(1)$ and most theoretical models developed for weakly nonlinear waves are often inapplicable, as pointed out, for example, by Helfrich & Melville (2006). Although the fully nonlinear hydrodynamic equations (the Navier–Stokes equations) should be solved, they are computationally too expensive to describe the evolution of such strongly nonlinear long waves over a large area and a reduced model should therefore be adopted for real applications.

It has been shown that the strongly nonlinear long-wave models (Miyata 1988; Choi & Camassa 1999) for a two-layer system obtained without the classical small-amplitude assumption is a good approximation to the Euler equations even for the strongly nonlinear regime as long as its travelling wave solutions are concerned (Camassa *et al.* 2006). The model also shows excellent agreement with laboratory experiments of Michallet & Barthelemy (1998) and Grue *et al.* (1999) for the shallow

† Email address for correspondence: wychoi@njit.edu

and deep water configurations, respectively. The shallow configuration model is further generalized to a multi-layer system (Choi 2000) including the effects of bottom topography and the top free surface.

Despite their success in describing travelling solitary wave solutions, the strongly nonlinear models have not been used much to solve time-dependent internal wave problems. In particular, a major difficulty in solving numerically the strongly nonlinear model for the shallow configuration is that, regardless of the wave amplitude, the model suffers from the local Kelvin–Helmholtz (KH) instability associated with the velocity discontinuity across the interface, as shown in Jo & Choi (2002). Although no background shear is present when the interface is flat, a jump in tangential velocity is induced when the interface is deformed since the model was derived under the inviscid assumption that requires only continuity of normal velocity. Unlike the classical KH instability, this velocity jump depends on the interfacial displacement and varies in space to reach a maximum value at a point where the maximal displacement occurs. Since this variation is in general slow for internal solitary waves, local stability analysis under the assumption that the velocity jump is locally constant (true for short waves that are most unstable) is found to be an effective tool in understanding the stability characteristics of large amplitude internal solitary waves, as confirmed with numerical simulations of the strongly nonlinear model in Jo & Choi (2002). We remark that this instability stems not from the long-wave approximation, but from the inviscid two-layer assumption. In fact, Grue *et al.* (1997) observed previously the KH instability when they solved the Euler equations for a two-layer system.

Considering that finite amplitude internal solitary waves have been observed in laboratory and field experiments with little sign of instability, the KH instability present in the strongly nonlinear model for arbitrarily small wave amplitudes should be unrealistic. In other words, the strongly nonlinear model fails to describe some physical effects in real experiments where finite amplitude internal solitary waves were observed.

While a two-layer system is considered to be a good approximation to a density profile with a thin transition layer where a sharp density variation occurs, the presence of the thin layer cannot be neglected. In fact, the thin layer is known to have a stabilizing effect on the shear flow induced by an internal solitary wave (Bogucki & Garrett 1993), possibly, up to a certain critical wave amplitude. Therefore, the effect of the thin transition layer needs to be included in the model. Beyond this critical amplitude, the horizontal velocity changes so rapidly that the Richardson number becomes locally smaller than 1/4. Then, the resulting shear flow could be unstable and the KH billows would appear in real experiments. Another physical process that the strongly nonlinear model fails to describe the suppression of unstable short wavelength disturbances is viscous dissipation. The viscous effect along with the effect of the transition layer should be incorporated into the strongly nonlinear model to contain the unrealistic KH instability, but it is a non-trivial task to model these effects in a way consistent with the long-wave approximation.

An alternative approach to remove the unrealistic KH instability in the strongly nonlinear model for wave amplitudes less than the critical value is to modify the dispersive behaviour of short waves. Jo & Choi (2008) showed that it is not necessary to describe the short-wavelength behaviour accurately as long as the solitary wave solutions are concerned. Jo & Choi (2008) applied a low-pass filter to remove unstable short waves and successfully simulated the propagation of a single solitary wave of large amplitude for a long time. This indicates that the solitary wave solution maintains its shape and speed reasonably well as long as the low-wavenumber modes

are well-preserved. While a numerical filter is found to be effective to eliminate the KH instability for the propagation of a single solitary wave, it is less useful for more general time-dependent problems since the choice of the cutoff wavenumber is arbitrary.

Recently, Nguyen & Dias (2008) derived a weakly nonlinear internal wave model valid near a depth ratio for which cubic nonlinearity is important and showed numerically that their time-dependent model written in terms of the horizontal velocities at the top and bottom boundaries can be integrated to describe the propagation and collision of weakly nonlinear internal solitary waves. They proposed a range of vertical levels to be used for a real linear dispersion relation in the absence of shear, but presented no analysis in the case when the wave-induced velocity jump is present. This is a generalization of the idea of Nwogu (1993) who first proposed to use the horizontal velocity at the vertical level where the difference between the wave speed of the Boussinesq model for surface waves and that of the Euler equations is minimized. This idea was also adopted by Bona, Chen & Saut (2002, 2004) to investigate the well-posedness of the Boussinesq-type equations for weakly nonlinear surface waves.

In this paper, we propose a regularized strongly nonlinear model that is asymptotically equivalent to the original model, but has a different dispersive behaviour for short waves. We show both analytically and numerically that the unrealistic KH instability is suppressed in the regularized model and large amplitude internal solitary waves are stable to perturbations of arbitrary wavelengths even in the presence of shear.

By summarizing briefly the previous results on shear instability of internal solitary waves in a two-layer system in § 2, we obtain a system of nonlinear evolution equations written in terms of the horizontal velocities at arbitrary depth levels in § 3. By carrying out local stability analysis in the presence of a velocity jump across the interface, it is shown that the top and bottom boundaries are the vertical levels that make the new system stable in the widest range of physical parameters. The new model is tested numerically in § 4.

2. Strongly nonlinear model and instability of solitary waves

Large amplitude internal solitary waves in a system of two constant density layers bounded by two flat rigid boundaries can be described by the following strongly nonlinear long-wave model (Miyata 1988; Choi & Camassa 1999) written in terms of the displacement of the interface ζ, the depth-averaged velocities $\overline{u}_i$ and the pressure P at the interface ($i = 1$ and 2 represent the upper and lower layers, respectively):

$$\eta_{i,t} + (\eta_i \, \overline{u}_i)_x = 0, \tag{2.1}$$

$$\overline{u}_{i,t} + \overline{u}_i \, \overline{u}_{i,x} + g\zeta_x + \frac{P_x}{\rho_i} = \frac{1}{\eta_i}\left(\frac{1}{3}{\eta_i}^3 \, G_i\right)_x, \tag{2.2}$$

where g is the gravitational acceleration, ρ_i are the fluid densities with $\rho_1 < \rho_2$ for stable stratification and the subscripts x and t represent partial differentiation with respect to space and time, respectively. The local layer thicknesses η_i are defined by

$$\eta_1(x,t) = h_1 - \zeta(x,t), \quad \eta_2(x,t) = h_2 + \zeta(x,t), \tag{2.3}$$

and the model includes the nonlinear dispersive effects denoted by G_i

$$G_i = \overline{u}_{i,xt} + \overline{u}_i \, \overline{u}_{i,xx} - (\overline{u}_{i,x})^2. \tag{2.4}$$

We remark that the system approximates the Euler equations with errors of $O(\epsilon^4)$, where ϵ is the long-wave parameter defined by $\epsilon = h_1/\lambda$, and $h_2 = O(h_1)$ has been assumed. The system admits solitary wave solutions that can be found by solving a single first-order nonlinear ordinary differential equation for ζ reduced from (2.1) and (2.2), as shown in Choi & Camassa (1999). Unfortunately, when their dynamics are studied numerically, these solitary waves suffer from the local KH instability due to a velocity discontinuity across the interface (Jo & Choi 2002). This velocity jump is induced when the interface is displaced from its equilibrium position, and disappears when the interface becomes flat. The maximum velocity jump across the interface occurs at a point of maximal interfacial displacement and is given by

$$U_2 - U_1 = \frac{ca(h_1 + h_2)}{(h_1 - a)(h_2 + a)}, \tag{2.5}$$

where U_1 and U_2 are the horizontal velocities in the upper and lower layers, and a is the wave amplitude that is, for example, negative for a solitary wave of depression. The wave speed c is given by

$$\frac{c^2}{{c_0}^2} = \frac{(h_1 - a)(h_2 + a)}{h_1 h_2 - (c_0^2/g)a}, \quad {c_0}^2 = \frac{g h_1 h_2 (\rho_2 - \rho_1)}{\rho_1 h_2 + \rho_2 h_1}, \tag{2.6}$$

where c_0 is the linear long-wave speed. By assuming that the velocity jump varies slowly in space and can be considered locally constant, it can be shown (Jo & Choi 2002) that the solitary wave of amplitude a is stable only if

$$(U_2 - U_1)^2 \leqslant \frac{g(\rho_2 - \rho_1)[\rho_1(h_2 + a)\,\theta_1 + \rho_2(h_1 - a)\,\theta_2]}{\rho_1 \rho_2\, \theta_1 \theta_2}, \tag{2.7}$$

where $U_2 - U_1$ is given by (2.5) and θ_i are defined by

$$\theta_1 = 1 + \tfrac{1}{3}k^2(h_1 - a)^2, \quad \theta_2 = 1 + \tfrac{1}{3}k^2(h_2 + a)^2. \tag{2.8}$$

From (2.5) and (2.7), for any fixed wave amplitude, it is always possible to find a critical wavenumber k_{cr} beyond which the solitary wave is unstable to short-wave disturbances of $k > k_{cr}$, as shown in figure 4(*b*) in Jo & Choi (2002). Unless these unstable short waves are contained, the long-wave model given by (2.1) and (2.2) is ill-posed and has limited applicability.

3. Derivation of a regularized model

Under the long-wave approximation, the horizontal velocities $u_i(x, z, t)$ can be expressed (Whitham 1974, § 13.11) as

$$u_i(x, z, t) = u_i^{(0)}(x, t) - \tfrac{1}{2}(z \mp h_i)^2 u_{i,xx}^{(0)} + O(\epsilon^4), \tag{3.1}$$

where the minus and plus signs are chosen for $i = 1$ and 2, respectively. From the definition of the depth-mean horizontal velocities

$$\overline{u}_1(x, t) = \frac{1}{\eta_1}\int_{\zeta}^{h_1} u_1(x, z, t)\,\mathrm{d}z, \qquad \overline{u}_2(x, t) = \frac{1}{\eta_2}\int_{-h2}^{\zeta} u_2(x, z, t)\,\mathrm{d}z, \tag{3.2}$$

$\overline{u}_i$ can be written as

$$\overline{u}_i(x, t) = u_i^{(0)}(x, t) - \tfrac{1}{6}{\eta_i}^2 u_{i,xx}^{(0)} + O(\epsilon^4), \tag{3.3}$$

where η_i is defined in (2.3). On the other hand, from (3.1), the horizontal velocities evaluated at fixed vertical levels ($z=\hat{z}_1$ and $z=-\hat{z}_2$), $\hat{u}_i$ are given by

$$\hat{u}_i(x,t) = u_i^{(0)}(x,t) - \tfrac{1}{2} H_i{}^2 u_{i,xx}^{(0)} + O(\epsilon^4), \tag{3.4}$$

where

$$H_i = h_i - \hat{z}_i, \quad \hat{u}_1(x,t) = u_1(x, z=\hat{z}_1, t), \quad \hat{u}_2(x,t) = u_2(x, z=-\hat{z}_2, t), \tag{3.5}$$

with $0 \leqslant \hat{z}_i \leqslant h_i$. Then, the depth-mean velocities $\bar{u}_i$ are related to $\hat{u}_i$ by the following relation:

$$\bar{u}_i = \hat{u}_i - \tfrac{1}{6} \eta_i{}^2 \hat{u}_{i,xx} + \tfrac{1}{2} H_i{}^2 \hat{u}_{i,xx} + O(\epsilon^4). \tag{3.6}$$

By substituting (3.6) for $\bar{u}_i$ into (2.1) and (2.2) and neglecting terms of $O(\epsilon^4)$ or higher, (2.1) and (2.2) yield a new system of nonlinear evolution equations for η_i, $\hat{u}_i$ and P:

$$\eta_{i,t} + \left[\eta_i \left(\hat{u}_i - \tfrac{1}{6} \eta_i{}^2 \hat{u}_{i,xx} + \tfrac{1}{2} H_i{}^2 \hat{u}_{i,xx}\right)\right]_x = 0, \tag{3.7}$$

$$\hat{u}_{i,t} + \hat{u}_i \hat{u}_{i,x} + g\zeta_x + \frac{P_x}{\rho_i} = \left[\frac{1}{2} \eta_i{}^2 \left(\hat{u}_{i,xt} + \hat{u}_i \hat{u}_{i,xx} - \hat{u}_{i,x}^2\right)\right]_x - \frac{1}{2} H_i{}^2 (\hat{u}_{i,xt} + \hat{u}_i \hat{u}_{i,xx})_x, \tag{3.8}$$

where we have used $\eta_{it} = -(\eta_i \hat{u}_i)_x + O(\epsilon^2)$ to find the right-hand side of (3.8). Notice that the system given by (3.7) and (3.8) has an error of $O(\epsilon^4)$ and is, therefore, asymptotically equivalent to the original system (2.1) and (2.2).

3.1. *Linear dispersion relation in the absence of a velocity jump*

When linearized about $\eta_i = h_i$ and $\hat{u}_i = 0$, the new system (3.7) and (3.8) becomes

$$\mp\zeta_t + h_i \hat{u}_{i,x} + \alpha_i h_i{}^3 \hat{u}_{i,xxx} = 0, \tag{3.9}$$

$$\hat{u}_{i,t} + \alpha_i h_i{}^2 \hat{u}_{i,xxt} + g\zeta_x + \frac{P_x}{\rho_i} = \frac{1}{3} h_i{}^2 \hat{u}_{i,xxt}, \tag{3.10}$$

where the minus (or plus) sign is taken for $i=1$ (or $i=2$), and α_i is defined as

$$\alpha_i = \frac{1}{2}\left(\frac{\hat{z}_i}{h_i} - 1\right)^2 - \frac{1}{6}. \tag{3.11}$$

Notice that α_i decreases monotonically as $\hat{z}_i/h_i$ increases from 0 to 1 (equivalently, the vertical levels of choice move from the undisturbed interface with $\hat{z}_i = 0$ to the rigid boundaries with $\hat{z}_i = h_i$) so that

$$-\tfrac{1}{6} \leqslant \alpha_i \leqslant \tfrac{1}{3}. \tag{3.12}$$

For example, $\alpha_i = -1/6$ if we choose the horizontal velocities at the upper and lower rigid boundaries ($\hat{z}_i = h_i$). It is interesting to notice that, when $\alpha_i = 0$ with $\hat{z}_i/h_i = (3-\sqrt{3})/3 \simeq 0.4227$, (3.9) and (3.10) become identical to the linearized system of the original model (2.1) and (2.2) although the nonlinear solutions of the two models should be different.

The choice of α_i can be made with various considerations. For example, as Nwogu (1993) suggested for surface gravity waves, it can be chosen to minimize the error of the linear dispersion relation of the long-wave model (3.9) and (3.10) from that of the full linear theory for a two-layer flow given (Lamb 1945, § 231) by

$$\omega^2 = \frac{gk(\rho_2 - \rho_1)}{\rho_1 \coth(kh_1) + \rho_2 \coth(kh_2)}, \tag{3.13}$$

where ω and k are the wave frequency and the wavenumber, respectively. Although the long-wave models describe poorly the linear dispersive behaviour of short waves, it is not so essential for large amplitude internal solitary waves to tune α_i to match the dispersion relation with that of the Euler equations since significant wave energy is contained in low-wavenumber modes, as demonstrated by comparing the solitary wave solutions of the model with the numerical solutions of the Euler equations (Camassa *et al.* 2006).

Another important consideration in choosing α_i is that the wave frequency ω must be real for all k, with any choice of physical parameters ρ_i and h_i, in the absence of any background shear (or velocity jump), as suggested by Nguyen & Dias (2008). We remark that both the original long-wave model (2.1) and (2.2) and the Euler equations have this property. By assuming $(\zeta, u_i, P) \sim \exp[\mathrm{i}(kx - \omega t)]$, the linear dispersion relation for (3.9) and (3.10) can be obtained as

$$\omega^2 = \frac{g(\rho_2 - \rho_1)k^2 h_1 h_2 \beta_1 \beta_2}{\rho_1 h_2 \beta_2 \gamma_1 + \rho_2 h_1 \beta_1 \gamma_2}, \tag{3.14}$$

where β_i and γ_i are defined by

$$\beta_i = 1 - \alpha_i k^2 h_i^2, \qquad \gamma_i = 1 - \left(\alpha_i - \tfrac{1}{3}\right) k^2 h_i^2. \tag{3.15}$$

For the wave frequency ω to be purely real for all k, the right-hand side of (3.14) has to be always positive. Notice that $\gamma_i > 0$ for all k since $\alpha_i \leqslant 1/3$, as shown in (3.12). Then, the right-hand side of (3.14) is always positive if β_i are positive for all k, which is satisfied when $\alpha_i \leqslant 0$. If at least one of α_i is positive, it can be shown that the positiveness of the right-hand side of (3.14) is not guaranteed for some physical parameters. Therefore, an admissible range of α_i for the wave frequency to be real *in the absence of velocity shear* for all k with any choice of any physical parameters is $-1/6 \leqslant \alpha_i \leqslant 0$, which means that the vertical levels $\hat{z}_i$ must lie between $(3 - \sqrt{3})h_i/3$ and h_i. This is consistent with the conclusion of Nguyen & Dias (2008) for their weakly nonlinear system. Furthermore, they chose $\alpha_i = -1/6$ for their numerical studies of the propagation and collision of solitary waves, but no explanation was given for this choice. In the following section, local stability analysis based on the new model given by (3.7) and (3.8) is presented to determine α_i, which stabilizes the model in the presence of shear, and the detailed local stability characteristics of large amplitude internal solitary waves of the regularized model are described.

3.2. *Local stability analysis in the presence of velocity discontinuity*

To investigate the *local* stability characteristics of internal solitary waves, the new system (3.7) and (3.8) has to be linearized about $\eta_1 = h_1 - a$, $\eta_2 = h_2 + a$ and $\hat{u}_i = U_i$, where a and U_i are the local-wave amplitude and the induced velocity by a solitary wave, respectively, that are assumed to be constant. We first consider the case of $U_i \neq 0$, but $a = 0$. The result can be easily extended to the case of $a \neq 0$ by replacing h_1, h_2, $\hat{z}_1$ and $\hat{z}_2$ by

$$h_1 \to h_1 - a, \quad h_2 \to h_2 + a, \quad \hat{z}_1 \to \hat{z}_1 - a, \quad \hat{z}_2 \to \hat{z}_2 + a. \tag{3.16}$$

By substituting into (3.7) and (3.8) $\eta_i = h_i + \zeta'$, $\hat{u}_i = U_i + \hat{u}_i'$ and $P = P'$ and assuming the prime variables are small, the system linearized about $u_i = U_i$, $\eta_i = h_i$ and $P = 0$ is given, after dropping the primes, by

$$\mp(\zeta_{i,t} + U_i \zeta_{i,x}) + h_i \hat{u}_{i,x} + \alpha_i {h_i}^3 \hat{u}_{i,xxx} = 0, \tag{3.17}$$

$$(\hat{u}_{i,t} + U_i \hat{u}_{i,x}) + \alpha_i {h_i}^2 (\hat{u}_{i,xxt} + U_i \hat{u}_{i,xxx}) + g\,\zeta_x + \frac{P_x}{\rho_i} = \frac{1}{3} {h_i}^2 (\hat{u}_{i,xxt} + U_i \hat{u}_{i,xxx}). \tag{3.18}$$

By substituting the travelling wave solutions of $(\zeta, u_i, P) \sim \exp[\mathrm{i}(kx - \omega t)]$ into (3.17) and (3.18), the linear dispersion relation between ω and k can be obtained by solving the following quadratic equation:

$$(\rho_1 h_2 \beta_2 \gamma_1 + \rho_2 h_1 \beta_1 \gamma_2)\,\omega^2 - 2k(\rho_1 h_2 \beta_2 \gamma_1 U_1 + \rho_2 h_1 \beta_1 \gamma_2 U_2)\,\omega + k^2\left(\rho_1 h_2 \beta_2 \gamma_1 U_1^{\,2} + \rho_2 h_1 \beta_1 \gamma_2 U_2^{\,2}\right) - (\rho_2 - \rho_1) g k^2 h_1 h_2 \beta_1 \beta_2 = 0, \quad (3.19)$$

where β_i and γ_i are defined in (3.15). For ω to be real for all possible ranges of physical parameters ρ_i and h_i, the discriminant of (3.19) has to be non-negative

$$\Delta = -\rho_1 \rho_2 h_1 h_2 \gamma_1 \gamma_2 \beta_1 \beta_2 (U_2 - U_1)^2 + g(\rho_2 - \rho_1) h_1 h_2 \beta_1 \beta_2 (\rho_1 h_2 \beta_2 \gamma_1 + \rho_2 h_1 \beta_1 \gamma_2) \geqslant 0. \quad (3.20)$$

Since α_i lies in $-1/6 \leqslant \alpha_i \leqslant 0$ from our consideration for real wave frequency in the absence of velocity shear, both β_i and γ_i are positive and, therefore, the stability condition of $\Delta \geqslant 0$ can be written as

$$(U_2 - U_1)^2 \leqslant \frac{g(\rho_2 - \rho_1)(\rho_2 h_1 \beta_1 \gamma_2 + \rho_1 h_2 \beta_2 \gamma_1)}{\rho_1 \rho_2 \gamma_1 \gamma_2} = g(\rho_2 - \rho_1)\left(\frac{h_1}{\rho_1}\frac{\beta_1}{\gamma_1} + \frac{h_2}{\rho_2}\frac{\beta_2}{\gamma_2}\right). \quad (3.21)$$

For $\alpha_i = 0$, we have $\beta_i = 1$ and $\gamma_i = 1 + (1/3)k^2 h_i^{\,2}$; then, inequality in (3.21) reduces to the stability criterion of the original model given by (2.7) when h_1 and h_2 are replaced by $h_1 - a$ and $h_2 + a$, respectively, as explained in (3.16).

We remark that, for fixed α_i ($\leqslant 0$) and given physical parameters (ρ_i , h_i), the right-hand side of (3.21) is a function of wavenumber k; more specifically, it depends on $f_i(k) \equiv \beta_i(k)/\gamma_i(k)$. Since $f_i(k)$ decreases monotonically from a maximum value of 1 at $k = 0$ to a minimum value of $\alpha_i/(\alpha_i - 1/3)$ as $k \to \infty$, the right-hand side of (3.21) becomes smaller as k increases and the stability condition becomes most stringent for short waves. For stability for all k, the minimum of the right-hand side of (3.21) that occurs as $k \to \infty$ has to be greater than $(U_2 - U_1)^2$. Therefore, the best possible scenario for stability is to choose α_i such that the minimum of $f_i(k)$ is as large as possible. This can be achieved when α_i is chosen to be

$$\alpha_i = -\tfrac{1}{6}, \quad (3.22)$$

with $\hat{z}_i = h_i$ from (3.11) since the minimum of $f_i(k)$ which is $\alpha_i/(\alpha_i - 1/3)$ decreases monotonically for $-1/6 \leqslant \alpha_i \leqslant 0$. This implies that the model should be written in terms of the horizontal velocities at the top and bottom rigid boundaries for stability. It should be pointed out that the system is always unstable for $\alpha_i = 0$ corresponding to the original model (2.1) and (2.2) since the minimum value of f_i is 0 and the stability condition (3.21) becomes $(U_2 - U_1)^2 \leqslant 0$, which does not hold.

For $\alpha_i = -1/6$, the minimum value of f_i is $1/3$ and the stability condition (3.21) becomes

$$(U_2 - U_1)^2 \leqslant \frac{g(\rho_2 - \rho_1)(\rho_2 h_1 + \rho_1 h_2)}{3\,\rho_1 \rho_2}. \quad (3.23)$$

If this inequality holds for a given velocity jump $U_2 - U_1$, the system written in terms of the velocities at the top and bottom boundaries is stable to perturbations of arbitrary wavenumbers k.

To include the effect of large amplitude interfacial displacement on the local thicknesses, we apply the transformation (3.16) to the right-hand side of (3.23) and, after substituting the expression for $U_2 - U_1$ given by (2.5), we get the following

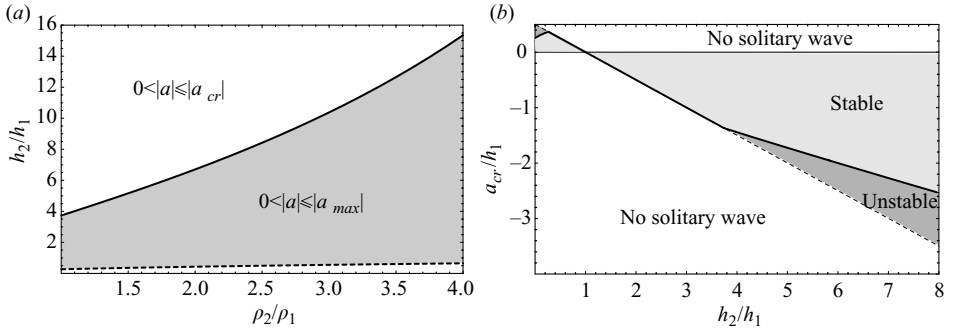

FIGURE 1. (*a*) Local stability characteristics of internal solitary waves: For $h\,(=h_2/h_1)$ and $\rho\,(=\rho_2/\rho_1>1)$ inside the shaded region, the solitary waves are stable for $|a|\leqslant|a_{max}|$ while they are stable for $|a|\leqslant|a_{cr}|<|a_{max}|$ elsewhere. The solid and dashed lines represent h^+ and h^-, respectively, that are the roots of the quadratic equation of (3.26), and a_{max} and a_{cr} are given by the equality of (3.24) and (3.25). (*b*) Critical wave amplitude a_{cr} for $\rho=1.003$. Solid line: a_{cr}; dashed line: a_{max}. Notice that $a_{cr}=a_{max}$ for $h^-\leqslant h\leqslant h^+$, where $h^-\simeq 0.2686$ and $h^+\simeq 3.7404$; otherwise, $|a_{cr}|<|a_{max}|$.

stability criterion for wave amplitude a:

$$3\rho_1\rho_2(h_1+h_2)^2a^2\leqslant(h_1-a)(h_2+a)[\rho_1(h_2+a)+\rho_2(h_1-a)]^2, \tag{3.24}$$

and the equality of (3.24) yields the critical wave amplitude a_{cr}. Then, the solitary wave is expected to become locally unstable to short waves when $|a|>|a_{cr}|$.

The solitary wave solutions of the original model (also the Euler equations) are known to exist up to the maximum wave amplitude a_{max} (Choi & Camassa 1999) given by

$$a_{max}=\frac{h_1\sqrt{\rho_2/\rho_1}-h_2}{\sqrt{\rho_2/\rho_1}+1}. \tag{3.25}$$

In order to find a domain of physical parameters (density and depth ratios) for which the internal solitary waves are stable for all possible wave amplitudes, we substitute (3.25) into (3.24) to have

$$(3-\sqrt{\rho}\,)h^2-8\sqrt{\rho}\,h+3\rho-\sqrt{\rho}\leqslant 0, \tag{3.26}$$

where ρ and h are the density and depth ratios, respectively, defined by $\rho=\rho_2/\rho_1>1$ and $h=h_2/h_1$. From (3.26), we can see that the maximum amplitude wave is stable if

$$h^-\leqslant h\leqslant h^+\quad\text{for } 1<\rho<9,\qquad h^-\leqslant h<\infty\quad\text{for } \rho\geqslant 9, \tag{3.27}$$

where $h^\pm$ are the roots of the quadratic equation for h in (3.26). For example, $h^-=2-\sqrt{3}\simeq 0.2679$ and $h^+=2+\sqrt{3}\simeq 3.7321$ in the limit of $\rho=1$; $h^-\to 1$ and $h^+\to\infty$ as $\rho\to 9$. As shown in figure 1(*a*), when the depth and density ratios h and ρ satisfy the condition given by (3.27), the solitary waves are stable for $0<|a|\leqslant|a_{max}|$; otherwise, the solitary waves are stable only for $0<|a|\leqslant|a_{cr}|<|a_{max}|$. In figure 1(*b*), for a small density ratio of $\rho=1.003$ relevant for oceanic applications, the critical wave amplitude is found to be the same as or close to a_{max} for all ranges of h. Compared with the original model given by (2.1) and (2.2) for which solitary waves of any amplitude are unstable to short waves, the regularized model improves greatly the stability characteristics of large amplitude internal solitary waves.

4. Numerical solutions of the regularized model

When we choose $\hat{z}_i = h_i$ corresponding to $\alpha_i = -1/6$, the system given by (3.7) and (3.8) reduces, with $H_i = 0$, to

$$\eta_{i,t} + \left[\eta_i \left(\hat{u}_i - \tfrac{1}{6}{\eta_i}^2 \hat{u}_{i,xx}\right)\right]_x = 0, \tag{4.1}$$

$$\hat{u}_{i,t} + \left(\frac{1}{2}\hat{u}_i^2 + g\zeta + \frac{P}{\rho_i}\right)_x = \left[\frac{1}{2}{\eta_i}^2\left(\hat{u}_{i,xt} + \hat{u}_i\hat{u}_{i,xx} - \hat{u}_{i,x}^2\right)\right]_x. \tag{4.2}$$

This is the regularized strongly nonlinear model for large amplitude internal solitary waves in a system of two layers bounded by the top and bottom rigid boundaries. This system is written in a conserved form and has two obvious conservation laws

$$\frac{\mathrm{d}}{\mathrm{d}t}\int_{-\infty}^{\infty} \zeta \,\mathrm{d}x = 0, \qquad \frac{\mathrm{d}}{\mathrm{d}t}\int_{-\infty}^{\infty} \hat{u}_i \,\mathrm{d}x = 0. \tag{4.3}$$

Since the system given by (4.1) and (4.2) has two degrees of freedom corresponding to the internal waves travelling to the right and to the left, respectively, as shown in (3.14), it is more convenient for numerical computations to solve (4.1) for $i = 1$ for ζ and the following system for $\hat{u}_1$ and $\hat{u}_2$:

$$\left[\eta_1 \left(\hat{u}_1 - \tfrac{1}{6}\,{\eta_1}^2 \hat{u}_{1,xx}\right)\right]_x + \left[\eta_2 \left(\hat{u}_2 - \tfrac{1}{6}\,{\eta_2}^2 \hat{u}_{2,xx}\right)\right]_x = 0, \tag{4.4}$$

$$\begin{aligned}&\rho_1\left[\hat{u}_{1,t} - \left(\tfrac{1}{2}{\eta_1}^2\hat{u}_{1,xt}\right)_x\right] - \rho_2\left[\hat{u}_{2t} - \left(\tfrac{1}{2}{\eta_2}^2\hat{u}_{2,xt}\right)_x\right] = (\rho_2 - \rho_1)g\zeta_x \\ &+ \rho_2\left[\tfrac{1}{2}\,\hat{u}_2^2 - \tfrac{1}{2}\,{\eta_2}^2\left(\hat{u}_2\hat{u}_{2,xx} - \hat{u}_{2,x}^2\right)\right]_x - \rho_1\left[\tfrac{1}{2}\,\hat{u}_1^2 - \tfrac{1}{2}\,{\eta_1}^2\left(\hat{u}_1\hat{u}_{1,xx} - \hat{u}_{1,x}^2\right)\right]_x,\end{aligned} \tag{4.5}$$

where the first and second equations are obtained by adding (4.1) for $i = 1$ and 2 to eliminate ζ_t and subtracting (4.2) multiplied by ρ_i for $i = 1$ and 2 to eliminate P, respectively. The system given by (4.4) and (4.5) is then solved numerically using the second-order central difference method in both space and time with the solitary wave solutions of the original system (2.1) and (2.2) as initial conditions.

After solving (4.1) for $i = 1$ for $\zeta^{(n+1)}$ at the new time level $n + 1$, we discretize the coupled equations (4.4) and (4.5) to find the following linear system for $\hat{u}_1^{(n+1)}$ and $\hat{u}_2^{(n+1)}$:

$$\begin{pmatrix} \boldsymbol{A} & \boldsymbol{B} \\ \boldsymbol{C} & \boldsymbol{D} \end{pmatrix} \begin{pmatrix} \hat{u}_1^{(n+1)} \\ \hat{u}_2^{(n+1)} \end{pmatrix} = \begin{pmatrix} b_1^{(n)} \\ b_2^{(n)} \end{pmatrix}, \tag{4.6}$$

where tridiagonal matrices $\boldsymbol{A}$, $\boldsymbol{B}$, $\boldsymbol{C}$ and $\boldsymbol{D}$ represent the discretized differential operators on the left-hand side of (4.4) and (4.5), and $b_1^{(n)}$ and $b_2^{(n)}$ denote the remaining parts of (4.4) and (4.5) that depend on ζ, $\hat{u}_1$ and $\hat{u}_2$ at the old time levels, n and $n - 1$.

In our computations, we set $h_1 = 1$ and $g = 1$ to fix length and time scales, and the length of the computational domain is $L = 200$. Typically, we choose $\Delta t = 0.1$ and $\Delta x = 200/1024 \approx 0.1953$ for time step and grid size, respectively. Since the initial condition that is the solitary wave solution of the original model (2.1) and (2.2) is expected to be close to, but not the exact solution of the regularized model (4.1) and (4.2), small amplitude disturbances are always generated and propagate towards one of the boundaries of the computational domain when the system is solved in a reference frame moving with the solitary wave speed. For example, for the right-going solitary wave, while the zero boundary condition is used at $x = L/2$, a radiation boundary condition is imposed at $x = -L/2$ by discretizing the following linearized Korteweg–de Vries equation in the reference frame moving with the solitary wave

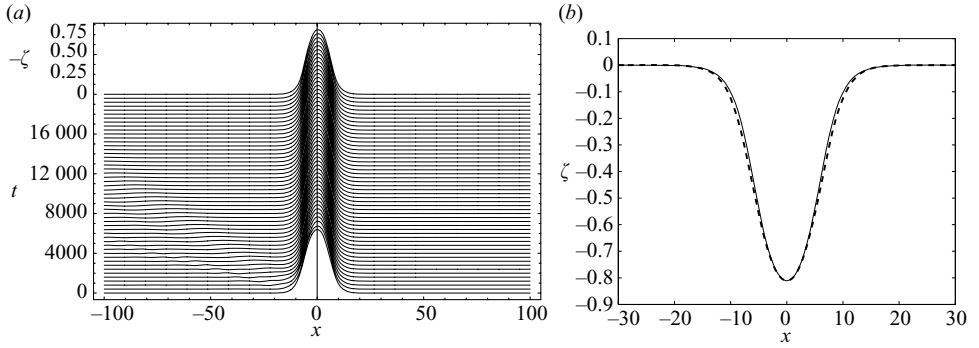

FIGURE 2. (*a*) Numerical solution of the regularized model (4.1) and (4.2) for $0 \leqslant t(g/h_1)^{1/2} \leqslant 2 \times 10^4$, initialized with a solitary wave solution of the original long-wave model (2.1) and (2.2) for $a/h_1 = 0.8$ ($a/a_{max} \simeq 0.8$), $h_2/h_1 = 3$ and $\rho_2/\rho_1 = 1.003$. (*b*) Comparison between the numerical solution of the regularized model (solid line) at $t(g/h_1)^{1/2} = 2 \times 10^4$ with the original solitary wave solution (dashed line).

speed $c\,(> 0)$:

$$\zeta_t - (c + c_0)\zeta_x - c_2\zeta_{xxx} = 0, \qquad c_2 = \frac{c_0}{6}\frac{\rho_1 h_1^2 h_2 + \rho_2 h_1 h_2^2}{\rho_1 h_2 + \rho_2 h_1}, \tag{4.7}$$

where $c_0\,(> 0)$ is defined in (2.6).

Figure 2 shows the numerical solution of the regularized model initialized with a single solitary wave solution of the original model (2.1) and (2.2) whose initial wave amplitude is a/h_1, about 80 % of the maximum amplitude $a_{max} \simeq -0.9985$. After small amplitude waves are shed and left the computational domain, the numerical solution reaches almost a steady state in a reference frame moving with the solitary wave speed $c \simeq 0.054$. Although the existence of solitary wave solutions of the regularized model is unknown, the computed wave profile at $t = 2 \times 10^4$ (or, equivalently, after the solitary wave travels about 5.45 times the computational domain) can be considered as an approximate solitary wave solution of the regularized model. It is interesting to notice that the numerical solution is very close to the solitary wave solution of the original model, as can be seen in figure 2(*b*). This implies that the regularized model is expected to serve as a model for large amplitude internal solitary waves as effectively as the original model. Since the density and depth ratios ($\rho_2/\rho_1 = 1.003$ and $h_2/h_1 = 3$) satisfy the condition given by (3.27), the solitary wave solution of the maximum amplitude which is a front solution should be stable. As shown in figure 3, the front remains to be stable, except for small amplitude waves shedding during the initial adjustment period, and stays close to the initial condition. On the other hand, for $h_2/h_1 = 5$, the critical wave amplitude is found, from (3.24), to be $a_{cr} \simeq -1.724$, which is less than the maximum wave amplitude $a_{max} \simeq -1.998$. As demonstrated in figure 4(*a*), when the wave amplitude ($a = -1.65$) is less than the critical amplitude, the numerical solution of the regularized model initialized with a solitary wave solution of the original model shows no sign of instability up to $t = 1.6 \times 10^4$ (or, equivalently, after the solitary wave travels about 5.33 times the computational domain). Notice that the solitary wave experiences slightly larger deformation from the initial profile than that for $h_2/h_1 = 3$ since the amplitude tested here is much larger. When $|a| > |a_{cr}|$, the KH instability appears quickly near the

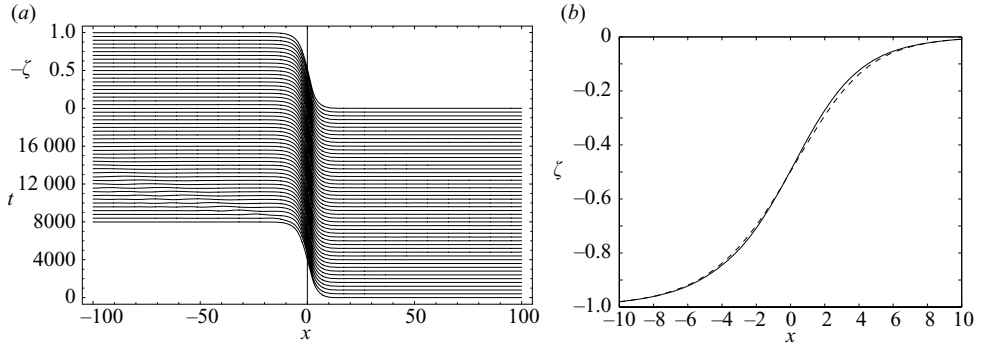

FIGURE 3. (*a*) Numerical solution of the regularized model (4.1) and (4.2) initialized with the front solution of the original long-wave model (2.1) and (2.2) for $a/h_1 \simeq 0.9985$ ($a/a_{max} = 1$), $h_2/h_1 = 3$ and $\rho_2/\rho_1 = 1.003$. (*b*) Comparison between the numerical solution of the regularized model (solid line) at $t(g/h_1)^{1/2} = 2 \times 10^4$ with the original front solution (dashed line).

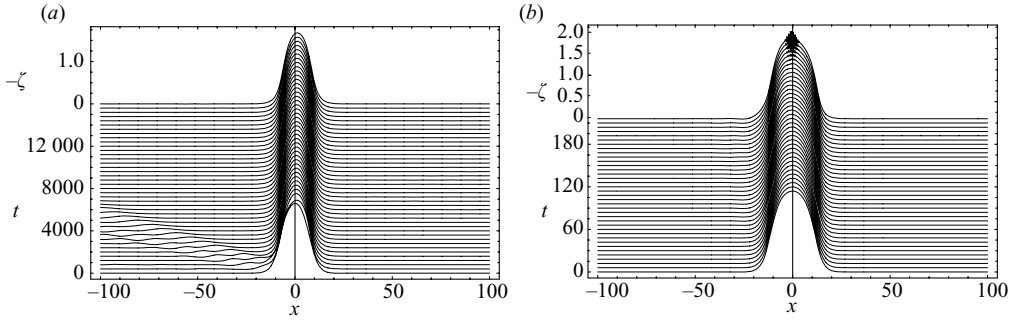

FIGURE 4. (*a*) Numerical solution of the regularized model (4.1) and (4.2) for $0 \leqslant t(g/h_1)^{1/2} \leqslant 1.6 \times 10^4$, initialized with a solitary wave solution of the original long-wave model (2.1) and (2.2) for $a/h_1 \simeq 1.65$ ($a/a_{max} \simeq 0.826$, $a/a_{cr} \simeq 0.957$), $h_2/h_1 = 5$ and $\rho_2/\rho_1 = 1.003$. (*b*) Numerical solution for $a/h_1 \simeq 1.9$ ($a/a_{max} \simeq 0.951$, $a/a_{cr} \simeq 1.102$). Since $|a| > |a_{cr}|$, the KH Instability appears near the location of the maximal displacement (or maximal shear), approximately, at $t(g/h_1)^{1/2} = 236$.

location of the maximal displacement where the maximum shear is induced, as shown in figure 4(*b*).

5. Concluding remarks

It is shown that, when the strongly nonlinear model for large amplitude internal solitary waves in a system of two layers of constant densities is written in terms of the horizontal velocities at the top and bottom boundaries, it suppresses unstable short waves excited by the KH instability mechanism in the original model. The critical wave amplitude below which internal solitary waves are stable is found to be close to the maximum wave amplitude for a wide range of parameters relevant for real applications in the ocean. The regularized model is then solved numerically using a finite-difference method and it is demonstrated that the regularized model stabilizes large amplitude internal solitary waves.

It is of interest to find how close the critical wave amplitude from our analysis of the regularized model is to the critical value measured in real experiments where

the two-layer approximation is almost valid. In principle, the regularized model should be used for solitary waves whose wave amplitudes are smaller than the experimentally measured critical wave amplitude. Although the KH instability is often observed locally near the crest of a large amplitude internal solitary wave, the unstable disturbances whose group velocity is smaller than the solitary wave speed often propagate away from the crest without destroying the solitary wave profile completely. Therefore, the regularized model might serve as an effective tool to study internal solitary waves even when their amplitudes are greater than the measured critical value.

It might not be so crucial to model the viscous effect on short waves accurately as far as the long-wave dynamics is concerned, but it is still instructive to examine the role of viscosity in containing unstable short waves in a two-layer system. For example, for a system of two immiscible fluids where the stabilizing effect of a thin transition layer is absent, our local stability analysis indicates that arbitrarily small amplitude interfacial solitary waves of the original inviscid system are unstable, which is unphysical. Therefore, viscosity should play a role in the determination of the onset of instability for such system.

It should be pointed out that our local stability analysis for uniform background shear provides an approximate estimate of the true stability criterion for internal solitary waves in a two-layer system. Although this approximate criterion is sufficient to derive a regularized model, a more comprehensive linear stability analysis for non-uniform background shear across the deformed interface is required to fully describe the stability characteristics of large amplitude internal solitary waves. Furthermore, the long-term evolution of unstable solitary waves leading to the KH billows cannot be addressed by the long-wave model, and the fully nonlinear hydrodynamic equations must be solved.

WC and RB gratefully acknowledge support from the US National Science Foundation through Grant No. DMS-0620832 and the US Office of Naval Research through Grant No. N00014-08-1-0377. The work of T-CJ was supported by the Inha University Research Grant INHA-35017.

REFERENCES

Bogucki, D. & Garrett, C. 1993 A simple model for the shear-induced decay of an internal solitary wave. *J. Phys. Oceanogr.* **23**, 1767–1776.

Bona, J. L., Chen, M. & Saut, J.-C. 2002 Boussinesq equations and other systems for small amplitude long waves in nonlinear dispersive media. I. Derivation and linear theory. *J. Nonlinear Sci.* **12**, 283–318.

Bona, J. L., Chen, M. & Saut, J.-C. 2004 Boussinesq equations and other systems for small amplitude long waves in nonlinear dispersive media. II. Nonlinear theory. *Nonlinearity* **17**, 925–952.

Camassa, R., Choi, W., Michallet, H., Rusas, P. & Sveen, J. K. 2006 On the realm of validity of strongly nonlinear asymptotic approximations for internal waves. *J. Fluid Mech.* **549**, 1–23.

Choi, W. 2000 Modelling of strongly nonlinear internal gravity waves. In *Proceedings of the Fourth International Conference on Hydrodynamics* (ed. Y. Goda, M. Ikehata & K. Suzuki), pp. 453–458.

Choi, W. & Camassa, R. 1999 Fully nonlinear internal waves in a two-fluid system. *J. Fluid Mech.* **396**, 1–36.

Grue, J., Friis, H. A., Palm, E. & Rusas, P. E. 1997 A method for computing unsteady fully nonlinear interfacial waves. *J. Fluid Mech.* **351**, 223–353.

Grue, J., Jensen, A., Rusas, P. E., & Sveen, J. K. 1999 Properties of large-amplitude internal waves. *J. Fluid Mech.* **380**, 257–278.

Helfrich, K. R. & Melville, W. K. 2006 Long nonlinear internal waves. *Annu. Rev. Fluid Mech.* **38**, 395–425.

Jo, T.-C. & Choi, W. 2002 Dynamics of strongly nonlinear solitary waves in shallow water. *Stud. Appl. Math.* **109**, 205–227.

Jo, T.-C. & Choi, W. 2008 On stabilizing the strongly nonlinear internal wave model. *Stud. Appl. Math.* **120**, 65–85.

Lamb, H. 1945 *Hydrodynamics.* Dover.

Michallet, H. & Barthélemy, E. 1998 Experimental study of interfacial solitary waves. *J. Fluid Mech.* **366**, 159–177.

Miyata, M. 1988 Long internal waves of large amplitude. In *Proceedings of the IUTAM Symposium on Nonlinear Water Waves* (ed. H. Horikawa & H. Maruo), Berlin: Springer–Verlag, pp. 399–406.

Nguyen, H. Y. & Dias, F. 2008 A boussinesq system for two-way propagation of interfacial waves. *Phys.* D **237**, 2365–2389.

Nwogu, O. 1993 Alternative form of Boussinesq equations for nearshore wave propagation. *J. Waterway, Port, Coastal, Ocean Engng* **119**, 618–638.

Whitham, G. B. 1974 *Linear and Nonlinear Waves.* Wiley.